Journal of The Electrochemical Society, 2026 **173** 072506

Effects of Surfactants on the Morphology and Structure of Antimony Nanowires Grown in Track-Etched Membranes

M. F. P. Wagner,[1,*,z] K.-H. Lin,[1,2] L. Herzog,[1,2] and M. E. Toimil-Molares[1,2,*]

[1]*GSI Helmholtz Center, Materials Research Department, Darmstadt 64291, Germany*
[2]*Technische Universität Darmstadt, Department of Materials and Earth Sciences, Darmstadt 64287, Germany*

Ion track-etched membranes are excellent templates for growing nanowires by electroplating, as the template route provides precise and independent control over key characteristics such as size, shape, crystallinity, and composition of the grown nanowires. Achieving high filling ratios of the pores is essential for the reliable fabrication of nanowire-based devices, yet this must be accomplished without compromising structural quality or functional properties. While surfactants have previously been employed to improve said filling rations by improving the wettability, they also influence parameters such as nucleation and growth speeds as well as morphology and crystal structure of deposited material, and their specific effects on nanowire crystallinity and growth remain less explored. Here, we investigate the influence of two surfactants, a nonionic surfactant (Brij 58) and an anionic surfactant (Dowfax 2A1), at concentrations up to 0.4 mol l^{-1} on the electrodeposition process, morphology, and crystallographic structure of Sb nanowires. Our results demonstrate that both surfactants significantly enhance the pore-filling ratio while reducing the crystallite size of the deposited material, without disrupting the preferred (012) crystal orientation. These findings provide valuable insights for optimizing nanowire growth and tailoring microstructural properties through surfactant-assisted electroplating.
 [DOI: 10.1149/1945-7111/ae573f]

Manuscript submitted November 27, 2025; revised manuscript received March 9, 2026. Published April 3, 2026.

Supplementary material for this article is available online

The combination of ion track-etched membranes and electroplating provides a powerful and highly controllable approach for fabricating nanowires. The method consists of two distinct stages, allowing independent control over key parameters such as size, shape, crystallinity, and composition of the nanowires. In the first stage, a polymer template for the growth of nanowires is fabricated by first irradiating up to 100 μm thick polymer foils with swift heavy ions. During the irradiation, each energetic ion creates an individual ion-damaged zone, called ion track, which afterwards is selectively etched into an open pore.[1] While the irradiation step defines the number of nanochannels and can be used to fabricate parallel channels or interconnected channel-networks, the etching step defines the geometry and size of the channels and enables the fabrication of nanochannels with aspect ratios up to 1000 with diameters down to 10 nm.[1,2] Additionally the method also allows to fabricate hierarchical structures through sequential irradiation and etching steps.[1,2] In the second stage the pores are filled with material, using several deposition techniques including methods like atomic layer deposition, electroless deposition and electroplating.[1–3] Electroplating is particularly versatile because the electrolyte composition can determine the deposited material, while temperature, applied current or potential and additives can be used to influence the growth dynamics and crystallization behavior, and the coulometric charge, which is usually controlled via the plating time, defines the resulting nanowire length.[1,2,4–9]

For future device applications, a high pore filling ratio of the templates and excellent reproducibility are crucial. One way to achieve this is to optimize the electroplating conditions, for example by applying pulsed plating in order to equalize growth in the different pores by reducing diffusion layer thickness and facilitating the exchange of gasses with the electrolyte, that are produced during secondary processes.[10,11] Another way is to employ additives such as surfactants. In the context of ion track-etched polymer templates, surfactants are sometimes introduced during the pore etching process in order to tailor the pore shape.[2,11,12] It was shown that surfactant molecules adsorb on the pore walls improving the wettability of the membranes in aqueous electrolytes, specially of those with interconnected and complex nanochannel networks.[2,10,13] The addition of Dowfax 2A1 was crucial for the successful homogeneous electroplating of Sb nanowire networks.[14] Surfactant molecules can also adsorb on the electrode surfaces.[15–17] At low concentrations, adsorbed surfactant molecules can physically block growth sites on the surface, forcing adions to deposit on more readily available spots, yielding deposits with smaller grain sizes.[15–17] At higher concentrations, surfactant molecules can form more dense layers or multilayers which generate a steric hindrance effect that generally decreases the rate of charge- and ion transfer across the electrode interface, slowing down the growth process. This more controlled and uniform deposition usually results in finer crystallization and smoother, more compact surfaces.[15–17] Depending on the specific orientation and packing of the surfactant molecules, they can also act as shape-directing agents, controlling the texture and preferred orientation of the deposited material.[15,17,18] While non-ionic surfactants like Brij 58 are less affected by the electrode charge or ions within the solution, anionic surfactants can further modify the electric double layer characteristics due to their charged head groups and can alter the local surface charge and potential and thereby affect reaction kinetics depending on the chemical environment.[15,17] By reducing the surface tension of the electrolyte, surfactants can also facilitate the transport of gases produced in secondary reactions away from the active surface, reduce internal stress of the deposits.[15,16] At very high concentrations, mesoporous deposits can be achieved when micelles, clusters of surfactant molecules, that can form once the surfactant concentration exceeds a critical micelle concentration (CMC), are enveloped by the growing material.[15–17,19–27]

Antimony (Sb) is of particularly interest as a model system for transport studies on low-dimensional materials like nanowires. Due to its Fermi wavelength of around 40 nm and a mean free path of charge carriers of a few microns, mesoscopic- and quantum size-effects due to geometrical confinement can be expected at already relatively large dimensions.[28–30] Quantum-size effects in combination with a larger contribution of surface states to transport at low-dimensions can potentially enhance the thermoelectric properties of Sb nanowires.[31–35] The thermal conductivity is expected be reduced compared to the bulk material, due to enhanced surface phonon scattering as was already observed for Sb thin films.[34,35] Furthermore, porosity introduced during electroplating in the presence of surfactants may further reduce the thermal conductivity due

*Electrochemical Society Member.
[z]E-mail: f.m.wagner@gsi.de

to additional scattering processes, enhancing its thermoelectric performance.[34] Sb nanowires with enhanced thermoelectric properties are promising candidates for applications in microscale quantum sensors.[36]

In this work, we investigate the effect of two surfactants - Dowfax 2A1 (anionic) and Brij 58 (nonionic) - on the electrochemical growth of parallel arrays of Sb nanowires. According to the manufacturer, the CMCs are approximately ∼0.012 mmol/100 g for Dowfax 2A1 in 1 M NaCl at 25 °C, and 0.007 mM for Brij 58 at the same temperature. The surfactant concentrations investigated in our experiments started at 0.02 mol l^{-1} for Dowfax 2A1 and 0.01 mol l^{-1} for Brij 58, both of which were well above their respective CMS. The resulting nanowires were characterized using scanning electron microscopy (SEM) and X-ray diffraction (XRD), to analyze their morphology and crystallographic structure.

Experimental

Template fabrication.—Templates were prepared by first irradiating circular polycarbonate foils (Makrofol N, diameter 30 mm, thickness 30 μm) with ∼2.2 GeV Au ions at the UNIversal Linear ACcelerator (UNILAC) at the GSI Helmholtz Center for Heavy Ion research in Darmstadt, Germany. Each foil was irradiated with $(1.5 \pm 0.5)\cdot 10^8$ ions cm^{-2}. Due to the high energy deposited by each individual ion along its trajectory, a latent track of structurally modified material, is generated. After irradiation, the foils were exposed to UV-light (T-30M Vilber Lourmat lamp, 30 W, 312 nm) for 1 h on each side. This treatment is known to narrow the pore diameter distribution after the subsequent etching process.[37–39] The latent tracks were then selectively etched by immersing the irradiated foils in 6 M NaOH solution (NaOH purity >= 98%) at 50 °C for 10 min, or for 3 min in the case of thinner-pore templates used for samples for transmission electron microscopy (TEM). These conditions usually yielded cylindrical pores with diameters of approximately 250 nm or 70 nm, respectively. After etching, the templates were rinsed several times in deionized (DI) water, stored in DI water for 24 h to remove residual NaOH from the pores, and finally air-dried. The average pore diameters measured by SEM after etching were 240±15 nm for the templates used for plating with Dowfax 2A1, and 280±25 nm for the plating with Brij 58. The larger pore diameter in the Brij 58 series was likely due to slightly higher temperatures of the NaOH bath during template etching.

Nanowire growth.—To establish electrical contact to the nanochannels, a ∼100 nm thick gold layer was first sputtered onto one side of each template, followed by electroplating an additional ∼3 μm thick Au layer to reinforce the contact. Gold electrodeposition was performed at room temperature (RT) using a two-electrode setup, with the sputtered Au layer acting as cathode (working electrode) and a Au spiral as anode (counter electrode). A constant current of −2.4 mA was applied using a GAMRY Reference 600 potentiostat. This additional electroplated Au layer sealed any remaining open pores to prevent electrolyte leakage during Sb nanowire deposition and guaranteed a good mechanical stability of the samples even after removal of the polymer matrix.

For the electroplating of Sb, an aqueous electrolyte containing 0.1 mol l^{-1} Sb(III)-chloride (analytical grade), 0.3 mol l^{-1} tartaric acid (99.5%), 0.2 mol l^{-1} NaCl (analytical grade), 1.95 mol l^{-1} HCl (99.5%), and 1.1 mol l^{-1} glycerol (99.5%) was used as the base solution. Either Dowfax 2A1 (anionic) or Brij 58 (nonionic) surfactant was added at specified concentrations. To deposit Sb into the templates a three-electrode configuration was employed, consisting of a $Pt_{80}Ir_{20}$ spiral counter electrode, a standard Ag/AgCl (saturated KCl) reference electrode (Sensortechnik Meinsberg), and the Au-back layer on the template as the working electrode. Electrodeposition was performed at a constant potential of U = −215 mV vs Ag/AgCl at room temperature (RT), while the current between working and counter electrodes was continuously recorded. Plating was terminated when a distinct current increase indicated cap formation at the pore openings, corresponding to complete nanowire growth.[1]

Sample characterization.—The morphology and crystallinity of the nanowires were examined by scanning electron microscopy (SEM), X-ray diffraction (XRD), and TEM. XRD measurements were carried out in Bragg-Brentano geometry with nanowires still embedded in the PC template. This allows to measure the crystal planes perpendicular to the nanowire axis. Powder diffraction data for Sb (JCPDS 35–732) was used to identify the observed reflections. For SEM and TEM, the polymer matrix was dissolved in multiple baths of dichloromethane (DCM). For TEM analysis, the nanowires were detached from the Au electrode via ultrasonication in solution and subsequently drop-casting the DCM/nanowire suspension onto Cu-lacey TEM grids.

Results and Discussion

Electroplating.—Representative I-vs-t curves measured during the potentiostatic electroplating with electrolytes containing various concentrations of Dowfax 2A1 or Brij 58 are shown in Figs. 1a and 1b, respectively. These curves display the typical behavior observed in nanowire plating in templates. Initially, a large current is recorded due to the polarization of the electrical double layer and the establishment of a diffusion zone. Following this, the current remains mostly stable as the pores are filled. The slight increase in current during this stage is likely due to the growth front approaching the pore mouth, which shortens the diffusion length for ions traversing from the pore mouth to the growth front. A significant current increase at the end of the plating occurs because growth is no longer limited by the pore dimensions when the material begins to grow out of the pores. This so-called cap growth leads to a rapid increase in the plating area, resulting in a corresponding rise in current.

Platings without a surfactant finish quickly, taking approximately 4 min to reach the top surface of the 30 μm thick template, which corresponds to a growth rate of about 7.5 μm min^{-1}. In contrast, the addition of a surfactant reduces the plating current and thus the growth rate. This effect does not appear to correlate linearly with surfactant concentration for either Dowfax 2A1 or Brij 58. For platings performed with 0.02 mol l^{-1} and 0.10 mol l^{-1} Dowfax 2A1, wire growth took about 10 min; however, the measure currents differed significantly, with the current for the 0.10 mol l^{-1} electrolytes being on average only about half that of the 0.02 mol l^{-1}. At higher concentrations of 0.20 mol l^{-1} and 0.40 mol l^{-1}, the plating time significantly increased to roughly 120 min, corresponding to a much slower growth rate of ∼0.25 μm min^{-1}. Notably, at the highest surfactant concentration investigated, no distinct current increase associated with cap growth was detected, even though surface caps were clearly visible on the samples. For Brij 58, changes in plating current and growth rate occur more gradually. While platings with Dowfax 2A1 at low concentrations are slightly faster than those with Brij 58, the highest Brij 58 concentration investigated (0.20 mol l^{-1}) required approximately 60 min to reach the surface, corresponding to an average growth rate of ∼0.5 μm min^{-1}, which is about twice that observed for Dowfax 2A1 under similar conditions.

It is worth noting that plating currents for the Brij 58 series were generally higher than those in the Dowfax 2A1 series, which is particularly evident when comparing platings without surfactant in both series. This discrepancy is likely caused by the approximately 40 nm larger pore diameter and the greater density of pores in the templates used for this series.

Figure S1 in the supplementary information (SI) shows a comparison of CVs for electrolytes containing no surfactant as well as the highest concentrations of Dowfax 2A1 and Brij 58 investigated in this study. Two cathodic peaks can be identified for the electrolytes. Based on the works of Vereecken et al. these can be attributed to a 2D nucleation and growth process and a bulk deposition process, which, for the electrolyte without any surfactant, are identified at around −140 mV and −240 mV vs Ag/AgCl,

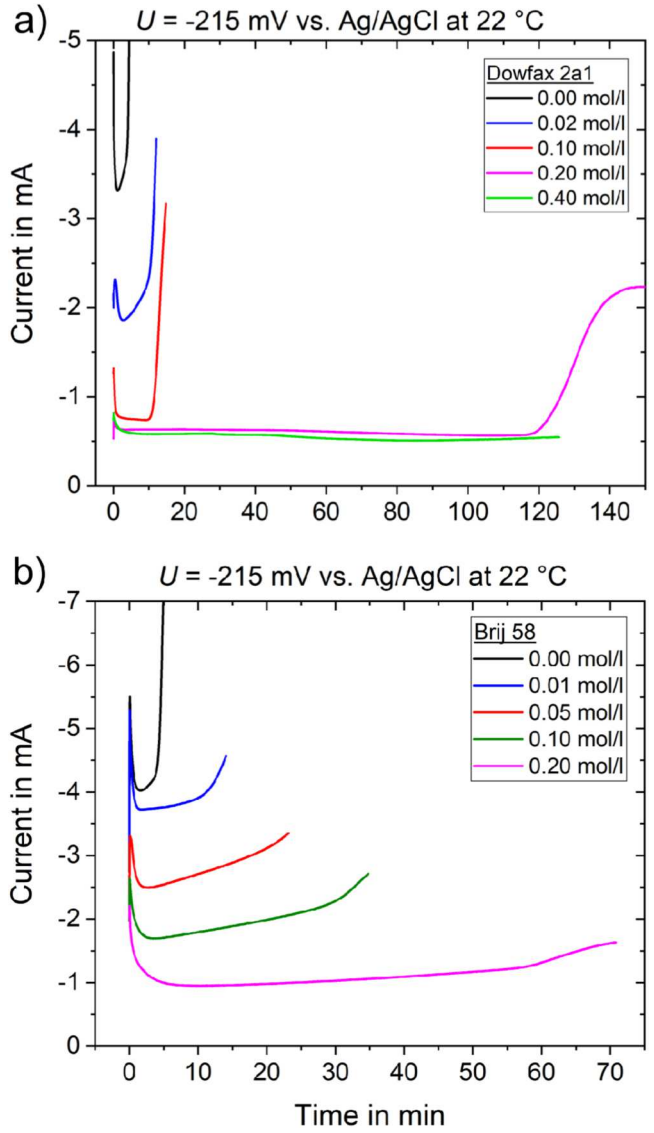

Figure 1. Representative I-vs-t curves during electroplating at a constant potential of −215 mV vs Ag/AgCl for (a) electroplating Sb into $1.3{\cdot}10^8$ pores cm^{-2} with a pore diameter of ∼240 nm, using electrolytes with various Dowfax 2A1 concentrations and (b) electroplating Sb into $2.2{\cdot}10^8$ pores cm^{-2} with a pore diameter of ∼280 nm, using electrolytes containing various Brij 58 concentrations.

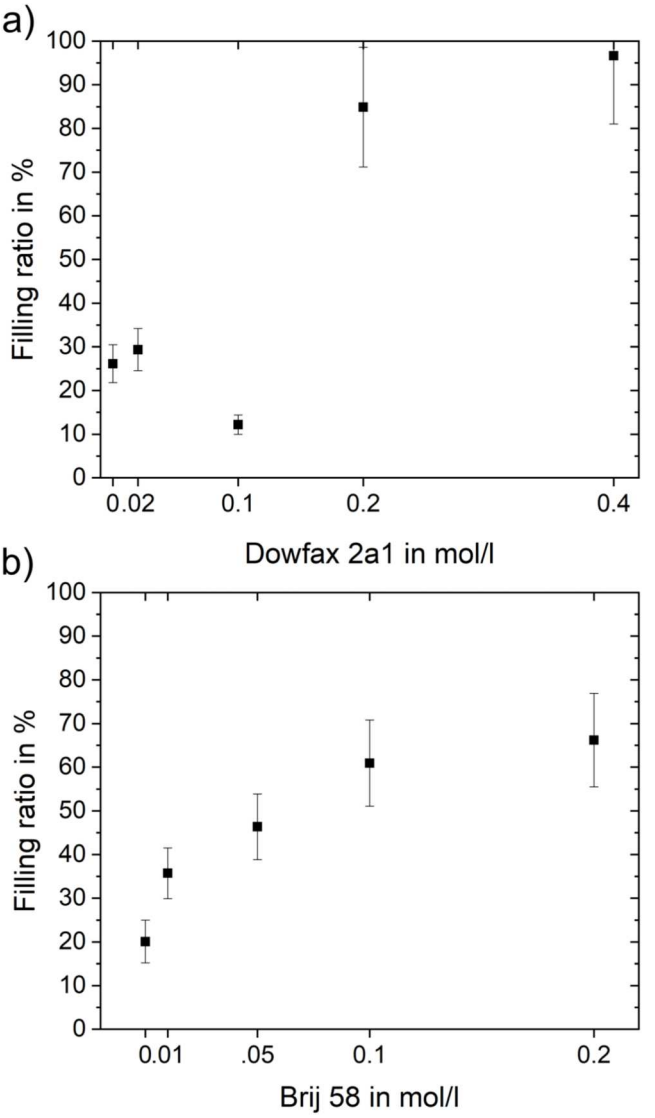

Figure 2. Average pore filling ratios of multiple platings after electroplating at a constant potential of −215 mV vs Ag/AgCl for (a) electroplating Sb into $1.3{\cdot}10^8$ pores cm^{-2} with a pore diameter of ∼240 nm, using electrolytes with various Dowfax 2A1 concentrations and (b) electroplating Sb into $2.2{\cdot}10^8$ pores cm^{-2} with a pore diameter of ∼280 nm, using electrolytes containing various Brij 58 concentrations.

respectively.[40] With the addition of surfactants, the onset and peak of the 2D nucleation process change only slightly. However, the bulk deposition process shows a more significant shift by ∼30 mV and ∼60 mV to more negative potentials for Dowfax 2A1 and Brij 58, respectively. This shift is likely caused by the formation of a surfactant layer on the electrode surface, which decreases the rate of charge and ion transfer across the electrode interface.[15–17] This potential shift also helps explain why the plating currents decrease with increasing surfactant concentrations. Additionally, the observed effects might be related to an increase in the viscosity of the electrolytes as surfactant concentration rise. For thin-layer electrodeposition, it was observed that higher viscosity results in reduced convection, an increase in cell voltage when constant currents are applied, and a general slowdown of all transport processes.[41] The precise effect of surfactant concentration on viscosity is difficult to establish, as the formation of micelles and their interactions lead to nonlinear dependence of viscosity on surfactant concentration, indicating a need for further research in this area.

Figure 2 displays the average template filling ratio as a function of surfactant concentration for (a) Dowfax 2A1 and (b) Brij 58. Without surfactant, only about 20%–25% of the pore volume was filled. The addition of small amounts of Dowfax 2A1 initially led to a slight improvement, but at 0.10 mol l^{-1}, the lowest filling ratio was consistently observed across multiple sample series. With further increase in concentration, the filling ratio rose sharply, reaching ∼85% at 0.20 mol l^{-1} and exceeding 95% at 0.40 mol l^{-1}. For Brij 58 the filling ratio of the pores increased more gradually with increasing concentration, seeming to reach a saturation at around 65% at the highest concentration tested.

Morphology.—Representative scanning electron microscopy (SEM) images of Sb nanowires, grown using electrolytes containing different concentrations of Dowfax 2A1, are shown in Fig. 3. Without surfactant, the nanowires exhibit a rough morphology and consist of relatively large crystallites that are not able to completely fill the pores during nanowire growth. This incomplete filling leaves a significant open volume, which explains the low filling ratios

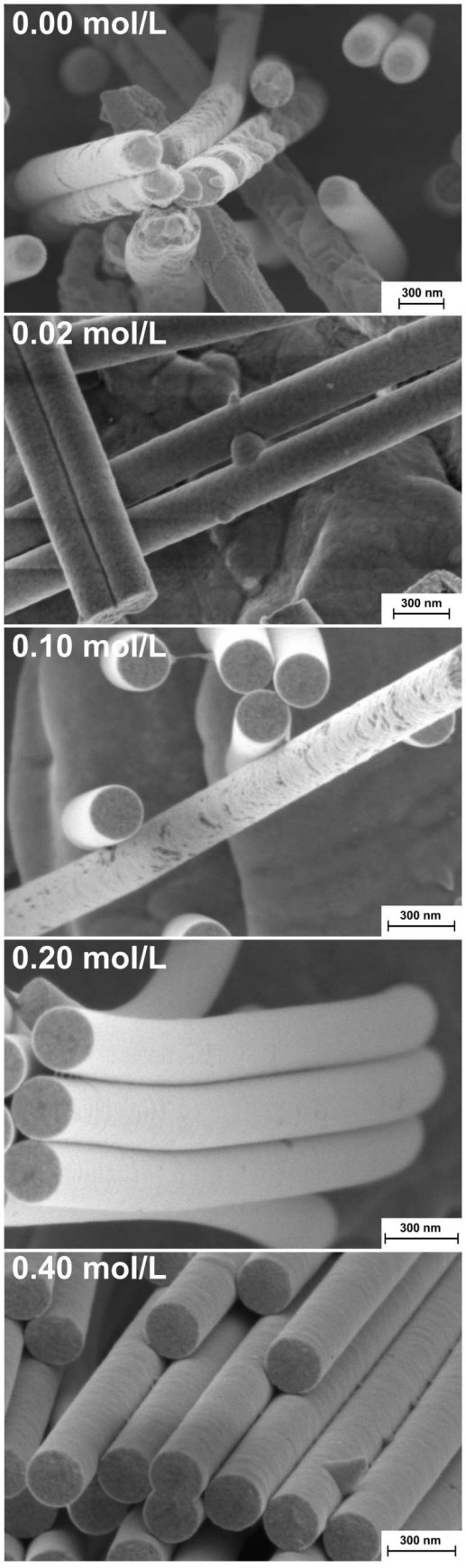

Figure 3. SEM images of Sb nanowires grown with electrolytes containing different concentrations of Dowfax 2A1, after removal of the polymer template.

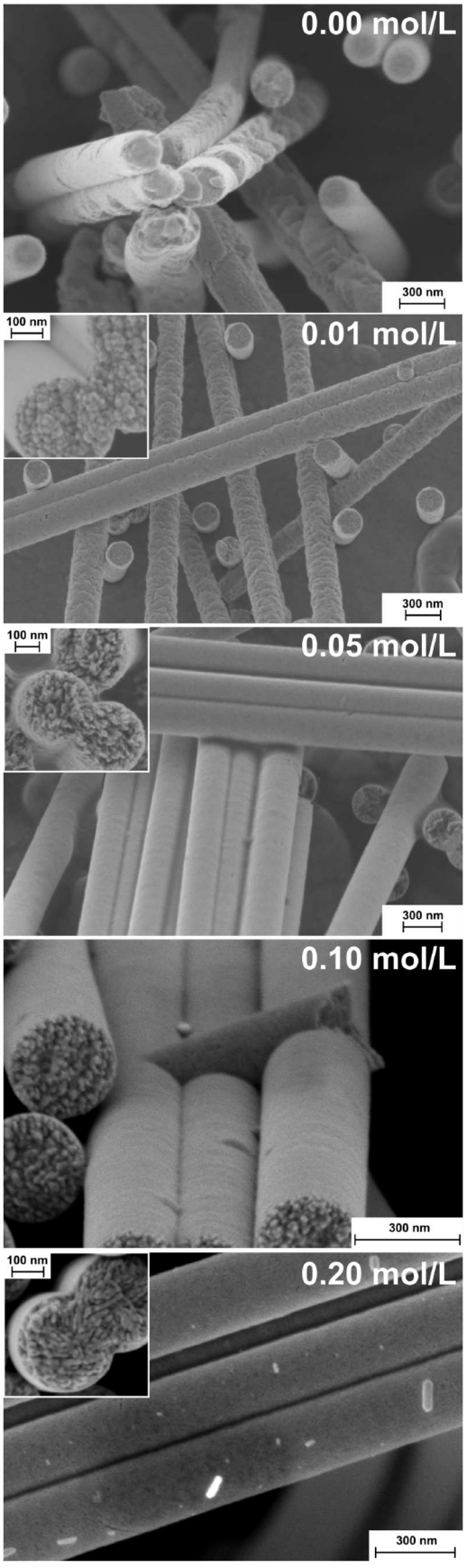

Figure 4. SEM images of Sb nanowires prepared with electrolytes containing different concentrations of Brij 58 after removal of the polymer template.

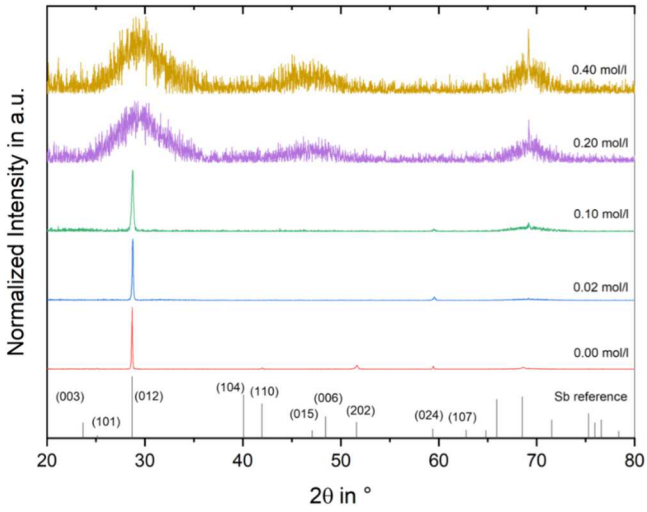

Figure 5. X-ray diffractograms of Sb nanowire arrays grown with electrolytes containing different Dowfax 2A1 concentrations (indicated on the right). For reference, the bottom of the graph shows position and relative intensities of reflections of a random oriented Sb powder sample (JCPDS 35–732).

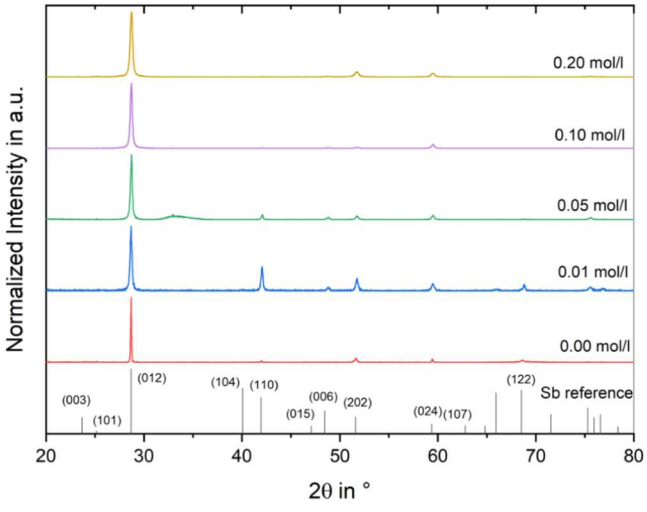

Figure 6. X-ray diffractograms of Sb nanowire arrays grown with electrolytes containing different Brij 58 concentrations (right). Peak positions and relative intensities of a reference Sb powder (JCPDS 35–732) are shown at the bottom.

obtained for samples prepared without surfactants. When surfactant-containing electrolytes were used, the nanowire surfaces appear noticeably smoother, and the wires appear to be composed of smaller, nearly spherical crystallites. This finer grain structure appears to promote more uniform deposition and facilitate pore filling. For electrolytes containing 0.02 mol l^{-1} Dowfax 2A1, the nanowire surfaces appear smoother than those grown with 0.10 mol l^{-1} surfactant. In the latter case, the wire surfaces display increasing porosity, which correlates with lower filling ratios observed for these samples. Although the nanowires appear to consist of smaller crystallites, similar in size to those grown with 0.02 mol l^{-1} Dowfax 2A1, the cause of the higher porosity remains unclear. Samples prepared with higher surfactant concentrations (0.20 mol l^{-1} and 0.40 mol l^{-1} Dowfax 2A1) consist of even smaller crystallites, producing smoother wires which further improving pore filling.

Figure 4 shows representative SEM images of Sb nanowires grown with electrolytes containing various Brij 58 concentrations. Insets in the upper left of some images show higher magnification views of the nanowire tips when not clearly visible in the main image. Similar to the Dowfax 2A1 series, the addition of Brij 58 to the electrolyte causes a significant grain refinement, leading to reduced surface roughness which explains the higher filling ratios. However, unlike the Dowfax 2A1-grown nanowires, the crystallites here exhibit a broader range of morphologies, including spherical, needle-like, and plate-like shapes, with no apparent systematic correlation to surfactant concentration. At the highest Brij 58 concentration (0.20 mol l^{-1}), the nanowire surfaces begin to exhibit increased porosity compared with samples at lower concentrations, likely due to the significantly elevated micelle concentration within the electrolyte.

Crystallinity.—Figure 5 shows the X-ray diffractograms (XRDs) of Sb nanowire arrays still embedded in the template material, fabricated using different concentrations of Dowfax 2A1 surfactant, with intensities normalized to the (012) reflexion. At the bottom of the graph, the reference positions and relative intensities of reflections for a randomly oriented Sb powder sample (JCPDS 35–732) are shown for comparison. Without any surfactant in the electrolyte, the Sb nanowires exhibit a pronounced (012) texture, which persists across all investigated surfactant concentrations. With increasing Dowfax 2A1 concentration, a slight reflection broadening appears, indicating a decrease in crystallite size already observed by SEM.[42] For surfactant concentrations of 0.20 mol l^{-1} and higher, the measured diffraction intensities significantly decrease, as seen from the increased signal-to-noise ratio. The broad intensity bands between approximately 25–35° and 42–50° can be attributed to the nanowire samples themselves, with the former likely corresponding to (012) planes. The pronounced broadening of these features indicates a very fine-grained and potentially even (partially) amorphous structure of the Sb nanowires when high Dowfax 2A1 concentrations are used. The broad reflection observed around 65–75° originates from the silicon sample holder. To further elucidate the crystallographic structure, 50 nm-diameter Sb nanowires prepared using 0.4 mol l^{-1} Dowfax 2A1 were examined by transmission electron microscopy (TEM) (see Figures S2 and S3 in the SI). The TEM data reveal small crystalline grains interspersed with large amorphous wire sections, confirming the XRD results. Notably, local recrystallization of the nanowires occurred under the electron beam, which may also explain the crystalline grains occasionally observed during TEM imaging. Thermal annealing of the nanowires embedded within the template at 130 °C for 3 h induced full recrystallization, restoring a strong (012) texture similar to that of nanowires grown at lower surfactant concentrations (see Fig. S4 in the SI). Longer annealing times did not lead to further structural changes.

Figure 6 shows the XRDs for samples prepared with Brij 58. The width of the (012) reflection increases only slightly with surfactant concentration, indicating that grain refinement occurs, but is less pronounced than in the Dowfax 2A1 series. Additional reflections besides the main (012) peak were occasionally observed, but no systematic correlation between their appearance and the Brij 58 concentration could be established.

Conclusions

We have reported the effects of the anionic surfactant Dowfax 2A1 and the nonionic surfactant Brij 58 on the electrochemical growth of Sb nanowires in ion track-etched polycarbonate membranes. When surfactants are added to the electrolyte and electroplating is performed at a constant potential of −215 mV vs Ag/AgCl, the deposition time increases with increasing surfactant concentration. This increase is gradual for Brij 58, whereas for Dowfax 2A1 a sharp rise in plating time occurs at concentrations at or above 0.20 mol l^{-1}. For Dowfax 2A1, only minor improvements in pore filling (∼25%) are observed at low concentrations, but a pronounced enhancement appears at and above 0.2 mol l^{-1}, where filling ratios reach up to 95%. This improvement correlates with a pronounced refinement of the crystal structure, from large grains to

nanocrystalline and partially amorphous structures, while maintaining a preferred (012) orientation along the wire axis. Surfactant addition suppresses coarse grain growth and promotes nucleation of smaller grains. This promotes a complete filling of the cylindrical channels and prevents the formation of large facetted single-crystalline sections, which reportedly result in nanowires displaying a rougher contour, resulting from merging of different crystal facets.[15–17] In the case of Brij 58, the filling ratio increases more gradually, from ∼25% without surfactant to ∼65% at 0.20 mol l^{-1}, and then tends to saturate. As with Dowfax 2A1, the improvement is attributed to grain refinement during growth, which promotes more uniform deposition and improved pore filling. Overall, both surfactants effectively enhance the filling of ion track-etched templates by promoting finer crystallite formation during electroplating. Future work will investigate how the surfactant concentration affected the viscosity of the electrolytes and to what extend this change contributed to the observed changes in structure and morphology. Furthermore, additional work investigating how the structural modifications influence the electrical and thermoelectrical transport properties of the resulting nanowires will be performed.

Acknowledgments

The nanowire samples were produced based on UMAT irradiations performed at the beam line X0 at the GSI Helmholtzzentrum für Schwerionenforschung, Darmstadt (Germany) in the frame of FAIR Phase-0.

The Authors thank W. Sigle and C. Schröck for their help in taking TEM images of the nanowires.

The publication is funded by the Deutsche Forschungsgemeinschaft (DFG, German Research Foundation)—491382106.

ORCID

M. F. P. Wagner https://orcid.org/0000-0002-2704-8413
K.-H. Lin https://orcid.org/0009-0009-7551-275X
L. Herzog https://orcid.org/0009-0007-4306-1400
M. E. Toimil-Molares https://orcid.org/0000-0002-3146-3193

References

1. M. E. Toimil-Molares, "Characterization and properties of micro- and nanowires of controlled size, composition, and geometry fabricated by electrodeposition and ion-track technology." *Beilstein J. Nanotechnol.*, **3**, 860 (2012).
2. M. F. P. Wagner, K.-O. Voss, C. Trautmann, and M. E. Toimil-Molares, "Three-dimensional nanowire networks fabricated by ion track nanotechnology and their applications." *EPJ Tech. Instrum.*, **10**, 2 (2023).
3. A. Spende et al., "TiO_2, SiO_2, and Al_2O_3 coated nanopores and nanotubes produced by ALD in etched ion-track membranes for transport measurements." *Nanotechnology*, **26**, 335301 (2015).
4. N. Ulrich, M. Schäfer, M. Römer, S. D. Straub, S. Zhang, J. Brötz, C. Trautmann, C. Scheu, B. J. M. Etzold, and M. E. Toimil-Molares, "Cu nanowire networks with well-defined geometrical parameters for catalytic electrochemical CO_2 reduction." *ACS Appl. Nano Mater.*, **6**, 4190 (2023).
5. M. Li, N. Ulrich, I. Schubert, W. Sigle, M. F. P. Wagner, C. Trautmann, and M. E. Toimil-Molares, "Three-dimensional free-standing gold nanowire networks as a platform for catalytic applications." *RSC Adv.*, **13**, 4721 (2023).
6. J. Krieg, *Characterization of Individual Bi2Te3 Nanowires Electrodeposited in Etched Ion-Track Membranes for Nano-ARPES and Electrical Transport Studies*, TU Darmstadt (2017), 10.26083/tuprints-00006750.
7. M. Rauber, I. Alber, S. Müller, R. Neumann, O. Picht, C. Roth, A. Schökel, M. E. Toimil-Molares, and W. Ensinger, "Highly-ordered supportless three-dimensional nanowire networks with tunable complexity and interwire connectivity for device integration." *Nano Lett.*, **11**, 2304 (2011).
8. T. da Câmara Santa Clara Gomes, J. De La Torre Medina, M. Lemaitre, and L. Piraux, "Magnetic and magnetoresistive properties of 3D interconnected NiCo nanowire networks." *Nanoscale Res. Lett.*, **11**, 466 (2016).
9. M. Schlesinger and M. Paunovic (ed), *Modern Electroplating* (John Wiley & Sons, Inc., Hoboken, New Jersey) 5 ed. (2010).
10. M. Cassinelli, S. Müller, Z. Aabdin, N. Perannio, O. Eibl, C. Trautmann, and M. E. Toimil-Molares, "Structural and compositional characterization of $Bi_{1-x}Sb_x$ nanowire arrays grown by pulsed deposition to improve growth uniformity." *Nucl. Instruments Methods Phys. Res. Sect. B Beam Interact. with Mater. Atoms*, **365**, 668 (2015).
11. W. E. G. Hansal and S. Roy, *Pulse Plating* (Eugen G. Leutze Verlag KG, Germany) (2012).
12. R. Spohr, C. Zet, B. E. Fischer, H. Kiesewetter, P. Apel, I. Gunko, T. Ohgai, and L. Westerberg, "Controlled fabrication of ion track nanowires and channels." *Nucl. Instrum. Methods Phys. Res. B*, **268**, 676 (2010).
13. P. Y. Apel, I. V. Blonskaya, S. N. Dmitriev, O. L. Orelovitch, A. Presz, and B. A. Sartowska, "Fabrication of nanopores in polymer foils with surfactant-controlled longitudinal profiles." *Nanotechnology*, **18**, 305302 (2007).
14. M. F. P. Wagner, F. Völklein, H. Reith, C. Trautmann, and M. E. Toimil-Molares, "Fabrication and thermoelectrical characterization of three-dimensional nanowire networks." *Phys. Status Solidi*, **213**, 610 (2016).
15. R. Vittal, H. Gomathi, and K.-J. Kim, "Beneficial role of surfactants in electrochemistry and in the modification of electrodes." *Adv. Colloid Interface Sci.*, **119**, 55 (2006).
16. T. C. Franklin and S. Mathew, "The use of surfactants in electrochemistry." *Surfactants in Solution* (Springer US)267 (1989).
17. F. Abouzeid and S. Alshammery, "Surfactants in electrochemical applications: a review." *GSC Adv. Res. and Rev.*, **22**, 151 (2025).
18. A. Biswal, B. C. Tripathy, T. Subbaiah, D. Meyrick, and M. Minakshi, "Dual effect of anionic surfactants in the electrodeposited MnO_2 trafficking redox ions for energy storage." *J. Electrochem. Soc.*, **162**, A30 (2015).
19. V. Malgras, H. Ataee-Esfahani, H. Wang, B. Jiang, C. Li, C.-W. Wu, J. H. Kim, and Y. Yamauchi, "Nanoarchitectures for mesoporous metals." *Adv. Mater.*, **28**, 993 (2016).
20. L. Oniciu and L. Mureşan, "Some fundamental aspects of levelling and brightening in metal electrodeposition." *J. Appl. Electrochem.*, **21**, 565 (1991).
21. K. Eiler, H. Krawiec, I. Kozina, J. Sort, and E. Pellicer, "Electrochemical characterisation of multifunctional electrocatalytic mesoporous Ni-Pt thin films in alkaline and acidic media." *Electrochim. Acta*, **359**, 136952 (2020).
22. J. Zhang, A. Quintana, E. Menendez, M. Coll, E. Pellicer, and J. Sort, "Electrodeposited Ni-based magnetic mesoporous films as smart surfaces for atomic layer deposition: An 'All-Chemical' deposition approach toward 3D nanoengineered composite layers." *ACS Appl. Mater. Interfaces*, **10**, 14877 (2018).
23. H. Chen, L. Hu, Y. Yan, R. Che, M. Chen, and L. Wu, "One-step fabrication of ultrathin porous nickel hydroxide-manganese dioxide hybrid nanosheets for supercapacitor electrodes with excellent capacitive performance." *Adv. Energy Mater.*, **3**, 1636 (2013).
24. P. N. Bartlett, B. Gollas, S. Guerin, and J. Marwan, "The preparation and characterisation of H1-e palladium films with a regular hexagonal nanostructure formed by electrochemical deposition from lyotropic liquid crystalline phases." *Phys. Chem. Chem. Phys.*, **4**, 3835 (2002).
25. K. Ariga, A. Vinu, Y. Yamauchi, Q. Ji, and J. P. Hill, "Nanoarchitectonics for mesoporous materials." *Bull. Chem. Soc. Jpn.*, **85**, 1 (2012).
26. K. Sai Jyotheender, M. K. Punith Kumar, and C. Srivastava, "Influence of surfactant polarity on the evolution of micro-texture, grain boundary constitution and corrosion behavior of electrodeposited Zn coatings." *Surf. Coatings Technol.*, **423**, 127594 (2021).
27. M. A. Malik, M. A. Hashim, F. Nabi, S. A. AL-Thabaiti, and Z. Khan, "Anti-corrosion ability of surfactants: A review." *Int. J. Electrochem. Sci.*, **6**, 1927 (2011).
28. J.-P. Issi, "Low temperature transport properties of the group V semimetals." *Aust. J. Phys.*, **32**, 585 (1979).
29. Y. Zhang, L. Li, G. H. Li, and L. D. Zhang, "Electrical transport properties of single-crystal antimony nanowire arrays." *Phys. Rev. B*, **73**, 113403 (2006).
30. J. Heremans, C. M. Thrush, Y.-M. Lin, S. B. Cronin, and M. S. Dresselhaus, "Transport properties of antimony nanowires." *Phys. Rev. B*, **63**, 085406 (2001).
31. L. D. Hicks and M. S. Dresselhaus, "Effect of quantum-well structures on the thermoelectric figure of merit." *Phys. Rev. B*, **47**, 12727 (1993).
32. L. D. Hicks and M. S. Dresselhaus, "Thermoelectric figure of merit of a one-dimensional conductor." *Phys. Rev. B*, **47**, 16631 (1993).
33. M. Cassinelli, S. Müller, K.-O. Voss, C. Trautmann, F. Völklein, J. Gooth, K. Nielsch, and M. E. Toimil-Molares, "Influence of surface states and size effects on the Seebeck coefficient and electrical resistance of $Bi_{1-x}Sb_x$ nanowire arrays." *Nanoscale*, **9**, 3169 (2017).
34. X. Cartoixà, R. Dettori, C. Melis, L. Colombo, and R. Rurali, "Thermal transport in porous Si nanowires from approach-to-equilibrium molecular dynamics calculations." *Appl. Phys. Lett.*, **109**, 013107 (2016).
35. F. Völklein and E. Kessler, "Thermal conductivity and thermoelectric figure of merit of thin antimony films." *Phys. Stat. Sol. (b)*, **158**, 521 (1990).
36. M. Lindeberg, H. Yousef, H. Rödjegård, H. Martin, and K. Hjort, "A PCB-like process for vertically configured thermopiles." *J. Micromechanics Microengineering*, **18**, 065021 (2008).
37. E. Ferain and R. Legras, "Heavy ion tracks in polycarbonate. Comparison with a heavy ion irradiated model compound (diphenyl carbonate)." *Nucl. Instruments Methods Phys. Res. Sect. B Beam Interact. with Mater. Atoms*, **82**, 539 (1993).
38. T. W. Cornelius, B. Schiedt, D. Severin, G. Pépy, M. Toulemonde, P. Yu Apel, P. Boesecke, and C. Trautmann, "Nanopores in track-etched polymer membranes characterized by small-angle X-ray scattering." *Nanotechnology*, **21**, 155702 (2010).
39. G. Pépy, P. Boesecke, A. Kuklin, E. Manceau, B. Schiedt, Z. Siwy, M. Toulemonde, and C. Trautmann, "Cylindrical nanochannels in ion-track polycarbonate membranes studied by small-angle X-ray scattering." *J. Appl. Crystallogr.*, **40**, s388 (2007).
40. P. M. Vereecken, S. Ren, L. Sun, and P. C. Searsonz, "Electrodeposition of $Bi_{1-x}Sb_x$ thin films." *J. Electrochem. Soc.*, **150**, C131 (2003).
41. G. Gonzalez, G. Marshall, F. V. Molina, S. Dengra, and M. Rosso, "Viscosity effects in thin-layer electrodeposition." *J. Electrochem. Soc.*, **148**, C479 (2001).
42. cf Holder and R. E. Schaak, "Tutorial on powder X-ray diffraction for characterizing nanoscale materials." *ACS Nano*, **13**, 7359 (2019).